Strongly Coupled Excitonic States in H-Aggregated Single Crystalline Nanoparticles of 2,5-Bis(4-methoxybenzylidene) Cyclopentanone

Qunling Fang,[†,‡] Feng Wang,[†,‡] Hui Zhao,[†] Xinran Liu,[†] Renyong Tu,[†] Dapeng Wang,[†] and Zhongping Zhang*[,†]

Key Laboratory of Biomimetic Sensing and Advanced Robot Technology, Institute of Intelligent Machines, Chinese Academy of Sciences, Hefei, Anhui 230031, China, and Department of Chemistry, University of Science and Technology of China, Hefei, Anhui 230026, China

Received: October 24, 2007; In Final Form: December 21, 2007

This paper reports that extremely strongly coupled excitonic states were formed in H-aggregated monocrystalline nanosheets and semicrystalline nanowires of coplanar organic molecules of 2,5-bis(4−methoxybenzylidene) cyclopentanone, due to the highly regular face-to-face stacking of molecular excitons. It was demonstrated that the spectral absorption and fluorescence emission behaviors are dependent on the routes of molecular aggregation and the ordered degree of molecular arrangement in aggregated nanoparticles. In particular, the H-type aggregation of molecules through a highly ordered molecular arrangement in the monocrystalline nanosheets led to the formation of a new exciton coupling state with an energy band higher than that in normal semi-/noncrystalline H-aggregation. A strong symmetric absorption at higher energy bands was thus observed in the solution of nanosheets. Furthermore, the strongly coupled excitonic state may hold all the oscillator strength, leading to the extinction of the original intramolecular electronic transitions of individual molecules and the appearance of new strong absorption and fluorescence emissions at high-energy bands. These results show a perspective that the ability to control the molecular structure and its arrangement in aggregates holds promise for creating novel optical properties in molecular materials.

Introduction

Tunable spectroscopic behaviors of organic molecular nanoparticles provide a wide range of versatility and flexibility inherent in their design and fabrication and therefore have attracted considerable research effort in enriching our understanding of their fundamental properties and enhancing their performance in practical applications.[1−4] The electronic properties of organic molecular nanoparticles are quite different from those of inorganic ones due to weak intermolecular forces such as hydrogen bonds, van der Waals forces, and hydrophilic/hydrophobic interactions. Depending on the fashions of molecular interactions and the methods of fabrication, J-aggregation with bathochromic shift absorption[4a,5] and H-aggregation with hypsochromic shift absorption were induced.[6,7] The routes of aggregation and the ordered degree of molecular arrangement in organic nanoparticles account for many unusual optical properties. Recently, J- and H-aggregated nanoparticles of various dye molecules have been prepared, and their effects of size and shape on optical properties have been studied widely.[3,4] In particular, for H-aggregates where molecules are aligned parallel to each other along the vertical axis of the molecular plane, the molecular orientation in aggregates may affect their optical behaviors greatly.[7] However, little attention was paid to the effect of the ordered degree of molecular arrangement on their optical behaviors. Therefore, the observation and understanding of the correlations between the aggregated regular degree of molecules and the optical behaviors of aggregates may further open up new opportunities to regulate the photophysical properties of organic molecular materials and provide new insights into the mechanism of molecular aggregation.

In principle, rigid backbone molecules with a totally coplanar π surface are expected to promote $\pi-\pi$ stacking,[8] thus enabling intermolecular electronic coupling and more efficient H-type aggregation. We thus synthesized a simple model molecule with a symmetric structure (2,5-bis(4-methoxybenzylidene) cyclopentanone (BMBCP)) as our compound. Small conjugation molecules are usually used as blocks for synthesizing larger conjugated systems.[9] Particularly, the BMBCP molecule has a coplanar preferential configuration due to the extension of intramolecular $\pi-\pi$ conjugation between two aromatic rings and cyclopentanone (Scheme 1), which is expected to provide feasibility for the formation of perfect H-type aggregates. In this work, H-aggregated materials of BMBCP were first prepared in the form of single-crystalline nanosheets and semicrystalline nanowires by reprecipitation and a melt-assisted template wetting method, respectively. We clearly demonstrated that the coupling strength of molecular excitons in H-aggregation depends on the regular degree of molecular exciton arrangements in aggregated nanostructures. It was found that extremely strongly coupled excitonic states were formed in the monocrystalline nanosheets and crystalline component of nanowires, due to the highly regular face-to-face stacking of coplanar molecules. The strong coupling of molecular excitons caused a new energy band that was much higher than that in the normal H-aggregation of the noncrystalline particles. The higher electronic state held all oscillator strength in the single crystalline nanosheets, leading to the extinction of the original intramolecular electronic transitions of the individual molecules. New absorption peaks and fluorescence emissions at higher energy

* Corresponding author. E-mail: zpzhang@iim.ac.cn.
† Chinese Academy of Sciences.
‡ University of Science and Technology of China.

10.1021/jp710262q CCC: $40.75
Published on Web 02/20/2008

SCHEME 1: Structure and Configuration of BMBCP Molecule

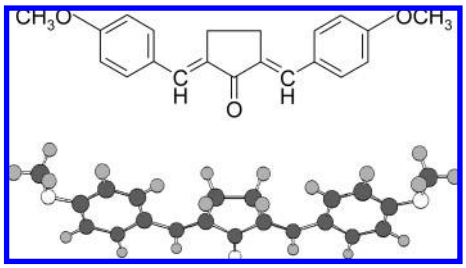

bands were thus induced. These were rarely observed in the previous research of H-aggregation.

Experimental Procedures

Materials. The model compound 2,5-bis(4-methoxybenzylidene)cyclopentanone (BMBCP) was synthesized by a one-step procedure as described previously.[9] Its structure was confirmed by nuclear magnetic resonance (NMR) and infrared (IR) spectroscopy. A yellow powder was obtained. Melting point: 210 °C. ^{1}H NMR ($CDCl_3$, ppm, TMS): δ 7.57 (d, 4H, Ar), 7.56 (S, CH, 2H), 6.97 (d, 4H, Ar), 3.86 (S, CH_3O, E), 3.81 (S, CH_3O, Z) 3.10 (S, CH_2, 4H). ^{13}C NMR ($CDCl_3$, ppm, TMS): 196.39, 160.67, 135.44, 133.42, 132.64, 128.92, 114.46, 114.44, 55.50, 26.60. IR (KBr, cm^{-1}): 3434, 1697, 1617, 1598, 1509, 1441, 1253, 1172, 1030, 836. Analytical grade acetone (Shanghai Chemicals Ltd.) and deionized water with a resistivity of 10 MΩ were used. The alumina membranes with pore diameters of ~70 nm were prepared by electrochemical anodization, according to the reported method in the literature.[10]

Synthesis of BMBCP Nanosheets. The organic BMBCP molecule is insoluble in water at room temperature. Thus, monocrystalline BMBCP nanosheets were readily prepared by reprecipitation in water through injecting 100 μL of a BMBCP/acetone stock solution (1.8×10^{-3} mol/L) into 10 mL of deionized water under rigorous stirring. The solution became rapidly turbid, and nanosheets began to form in the supersaturated system. After aging for 1 h, the resultant nanosheets were centrifuged and washed with water and were then redispersed in water for spectroscopic measurements.

Synthesis of BMBCP Nanowires. Semicrystalline BMBCP nanowires were prepared by a melt−assisted wetting method using a porous alumina membrane as the template.[11] Typically, the BMBCP powder was evenly cast on top of the porous alumina membranes with a pore diameter of ~70 nm, and then the alumina membranes were placed into a tubular furnace at 230 °C under argon atmosphere. This temperature is slightly higher than the melting point of BMBCP (210 °C). After the BMBCP powder melted for 30 min, the pores of the alumina membranes were filled with the melted BMBCP. After the alumina membranes were naturally cooled to room temperature, BMBCP nanowires were formed in the nanochannels of the porous alumina template by a melting-to-cooling procedure. Individual nanowires were obtained by mechanically polishing the surface of the alumina membranes with 3000 grid sand paper and then dissolving the alumina membranes with aqueous sodium hydroxide. The pure BMBCP nanowires were centrifuged, washed, and redispersed in water for spectroscopic measurements.

Characterizations. UV−vis absorption and steady-state fluorescence spectra were measured using aqueous dispersions of nanosheets and nanowires by a UNIC-4802 spectrometer and a Fluorolog-3-τ steady-state spectrofluorometer, respectively. The morphologies and structures of the nanoparticles were investigated using a FEI Sirion-200 field emission scanning electron microscope and a JEOL 2010 transmission electron microscope. The infrared spectra were recorded with a Nicolet Nexus-670 FT-IR spectrometer.

Results and Discussion

BMBCP is soluble in acetone and ethanol but not soluble in water. Single crystalline BMBCP nanosheets were readily prepared by reprecipitation in a poor solvent through simply injecting microamounts of the acetone solution into water under rigorous stirring. Figure 1A shows the SEM image of nanosheets deposited onto the silicon wafer. The thin nanosheets were inclined to lie flatly on the silicon substrate, and very sharp crystal faces can be recognized clearly. The selected area electron diffraction (SAED) pattern also exhibits a single−crystalline diffraction with a clear spot-like pattern (inset of Figure 1A). Therefore, these observations strongly confirm that the nanosheets are perfect single crystalline particles. Meanwhile, semicrystalline nanowires of BMBCP were successfully prepared by a melt-assisted template wetting procedure in alumina membrane pores. Figure 1B shows the SEM image of nanowires after the alumina template was removed by dissolving alumina using an aqueous NaOH solution. Individual nanowires were highly uniform in diameter (~70 nm) along its whole length, and the surface of the nanowires was very smooth as is shown in the TEM image of Figure 1B (inset). Although BMBCP is an easily crystallized ketone, the nanowires are still

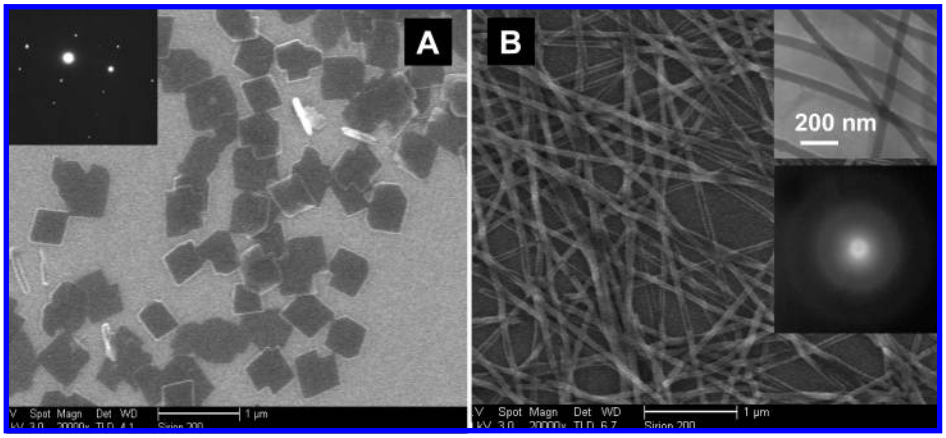

Figure 1. (A) SEM image and SAED pattern of single crystalline nanosheets and (B) SEM image of semicrystalline nanowires (insets are TEM image and SAED pattern of nanowires, respectively).

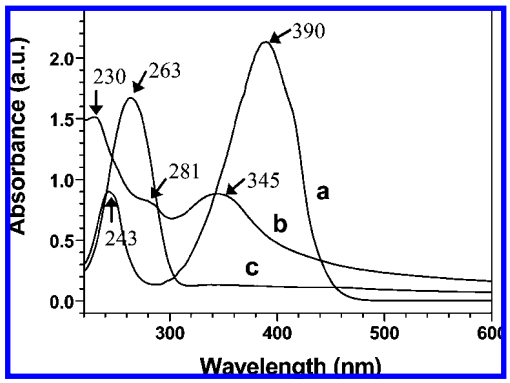

Figure 2. Absorption spectra of (a) monomers in ethanol, (b) nanowire, and (c) nanosheet dispersions in water. The concentration of BMBCP monomers in ethanol is 1.8×10^{-5} mol/L.

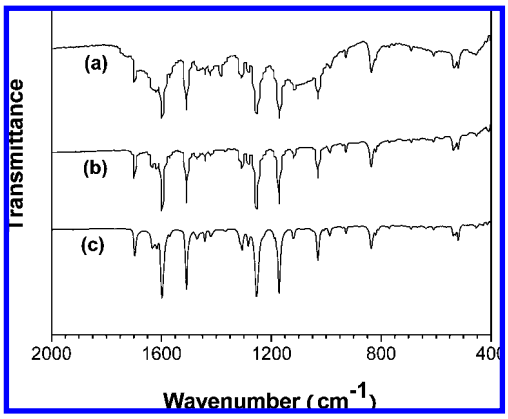

Figure 3. IR spectra of (a) nanosheets, (b) nanowires, and (c) powder of BMBCP.

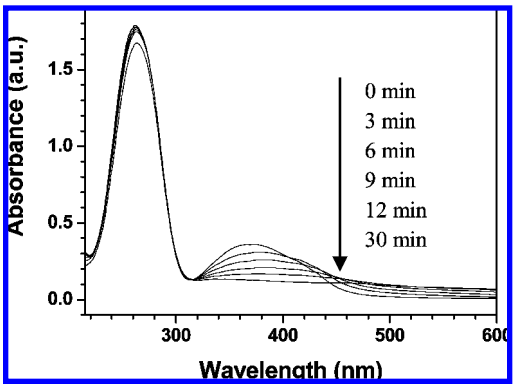

Figure 4. Evolution of absorption spectra of nanosheets with different aging times in water.

semicrystalline due to the fast melting-to-cooling process and the spatial restriction of the nanochannels of the alumina templates. The SAED shows a set of weak diffraction rings, suggesting a low crystalline degree of nanowires (inset SAED image in Figure 1B).

Figure 2a shows the absorption spectrum of BMBCP monomers in dilute solution. The monomer presents two intramolecular transition bands with λ_{max} at 243 nm from the phenyl ring (B_{phenyl}) and λ_{max} at 390 nm from the intramolecular $\pi-\pi^*$ transition ($B_{\pi-\pi^*}$), respectively. In the absorption spectrum of semicrystalline BMBCP nanowires, the B_{phenyl} and $B_{\pi-\pi^*}$ bands appear at 230 and 345 nm, respectively, as shown in Figure 2b. It can be observed that the λ_{max} values of $B_{\pi-\pi^*}$ and B_{phenyl} exhibit monotonically a hypsochromic shift as great as 45 and 13 nm, respectively, with respect to the monomeric transitions. Meanwhile, the peak of the $B_{\pi-\pi^*}$ band at 345 nm is broadened in the sample of BMBCP nanowires. These clearly suggest that the nanowires were formed by the H-aggregation of BMBCP monomers due to the π stacking interaction.[12−14] Together with these hypsochromic absorptions, we observed a weak absorption band at 281 nm that was far from the blue-shifted $B_{\pi-\pi^*}$ at 345 nm. This new band (designated as B_c) was not detectable in the monomeric solution and thus was expected to originate from a new kind of aggregation of BMBCP molecules in the crystalline component of nanowires (designated as H^c). These observations may suggest the presence of two kinds of H-aggregations in the semicrystalline nanowires: normal H-aggregation of the noncrystalline component with a low ordered degree of molecular arrangement and another new H^c-aggregation of the crystalline one with a highly ordered degree of molecular arrangement. The assumption was further explored by the observation on the absorption spectrum of single-crystalline nanosheets (Figure 2c). Most interestingly, the nanosheet dispersion in water only exhibited one single symmetric absorption band at 263 nm, and the original intramolecular transition bands including B_{phenyl} and $B_{\pi-\pi^*}$ disappeared completely, as shown in Figure 2c. It can be seen that the highly symmetrical band is stronger and narrower, accompanied by a small blue-shift of 17 nm, with respect to the B_c band of the semicrystalline nanowires. By the comparison with the absorption spectra of monomers and nanowires, we can confirm that the strong absorption at the higher energy band does not result from the hypsochromicity of $B_{\pi-\pi^*}$ in normal H-aggregation. The highly ordered arrangement of monomeric molecules in single crystals may lead to the formation of an extra strongly coupled− excitonic state that holds all oscillator strength. Moreover, the energy level of the new coupled state in the H^c-aggregated crystals is much higher than that in the H-aggregated noncrystalline components. Thus, a single strong absorption peak at the higher energy band was observed in the single-crystalline nanosheets. By comparing the IR spectra of powder, nanowires, and nanosheets, intramoleuclar distortions and hydrogen bonds were not observed (Figure 3). Therefore, the large change in the optical properties of single crystalline sheets did not result from the bond distortions and the formation of hydrogen bonds.

To obtain a better understanding of the formation mechanism of H^c-aggregation, we monitored the temporal evolution of absorption spectra at early growth stages of nanosheets (Figure 4). At the initial stage of reprecipitation, the mixture solution exhibited a strong narrow absorption band at 263 nm and a broadening absorption band ($B_{\pi-\pi^*}$) with λ_{max} at 367 nm. In comparison with absorption spectrum of the monomeric solution, the broadening absorption band with a blue-shift of 23 nm should be attributed to the formation of small aggregates of monomeric molecules in the saturated solution phase. With the increase of aging time, the normal H-aggregation band gradually disappeared, and the base lines of the absorption at the longer wavelength edge became higher due to the Mie scattering from the formation of larger particles.[12,14a,15] This indicated that those small H-type aggregates with a low regular degree dissolved and transformed into the H^c-aggregated monocrystalline particles by an Ostwald ripening process during the aging period. The evolution of absorption spectra clearly demonstrates two different kinds of aggregations in the precipitating process: normal H-aggregation with a low coupled excitonic state and monocrystalline H^c-aggregation with an extremely strongly coupled excitonic state. The B_c absorptions in both nanowires and nanosheets should originate from the ordered $\pi-\pi$ stacking of molecules in the crystalline phase.

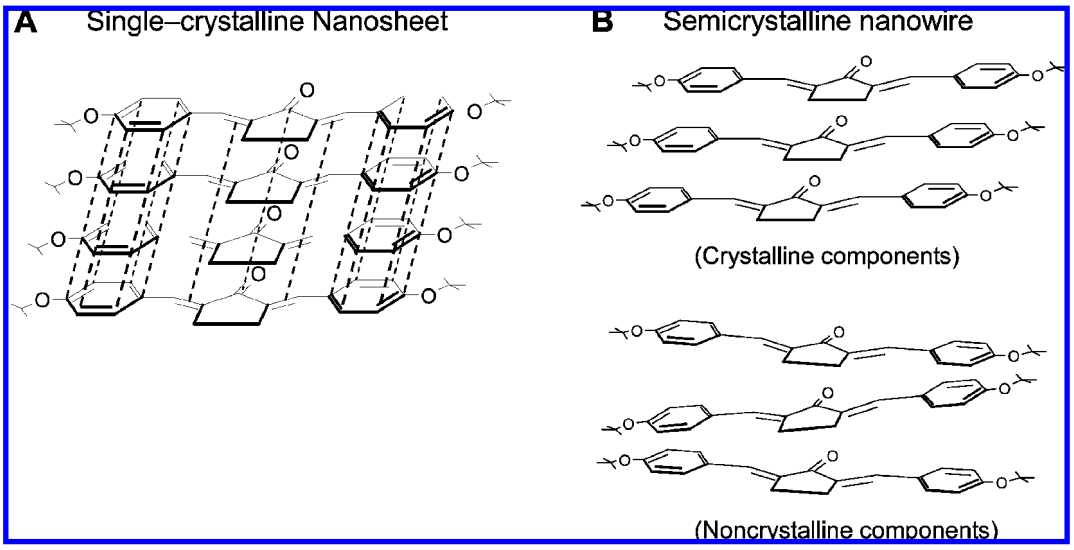

Figure 5. Schematic drawing for molecular aggregation in (A) single crystalline nanosheets and (B) semicrystalline nanowires including crystalline and noncrystalline components.

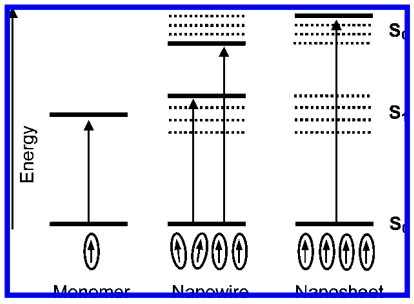

Figure 6. Schematic illustration for the arrangement of molecular excitons and the electronic transitions in monomers, semicrystalline nanowires, and monocrystalline nanosheets on the basis of the interaction of molecular excitons in aggregates (dashed lines represent the energy levels of forbidden transitions).

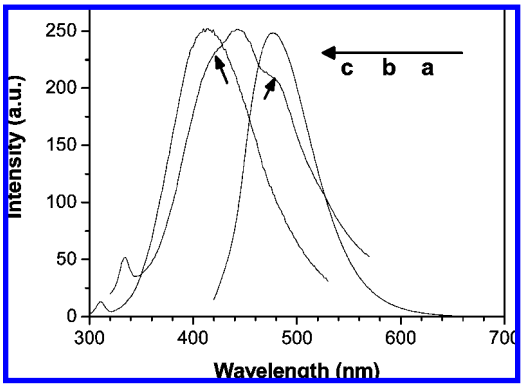

Figure 7. Normalized fluorescence emission spectra of (a) monomers in ethanol, (b) nanowire, and (c) nanosheet dispersions in water. The excitation wavelengths are 400, 300, and 280 nm, respectively.

Figure 5 illustrates the molecular arrangements in single crystalline nanosheets and semicrystalline nanowires. The BMBCP molecules in single crystalline nanosheets are arranged in very highly ordered $\pi-\pi$ stacking along the vertical axis of the molecular plane (Figure 5A), leading to the formation of extremely strong $\pi-\pi$ interactions. In the crystalline component of nanowires, the BMBCP molecules are also aligned in a parallel manner by $\pi-\pi$ stacking, as shown in Figure 5B. In the noncrystalline component of nanowires, however, the BMBCP molecules are aggregated in a low regular arrangement of molecules (Figure 5B), reducing the probability of a coupling interaction of $\pi-\pi$ stacking. Figure 6 illustrates the arrangement of molecular excitons and the electronic transitions in the monomer, semicrystalline nanowire, and single crystalline nanosheet on the basis of the interactions between molecular excitons in aggregates. The coplanar configuration of the BMBCP molecule enables it to easily stack along the vertical axis of the molecular plane in the aggregated state. In the case of nanowires, the molecular excitons are arranged in a low regular degree in the noncrystalline component, thus exhibiting the nature of normal H-aggregation. There, the electronic transition from the ground state to the highest energy level of the normal excited state will be induced (from S_0 to S_1). The absorption of the H-structure is thus blue-shifted, with respect to that of the monomeric solution, and is accompanied by the broadening of those blue-shifted peaks.[7,16] In the crystalline component of nanowires, however, these molecular excitons are arranged in a higher ordered manner, leading to the strong coupled− excitonic state due to the more regular face-to-face stacking. A new high-energy excited state (S_c) is formed in the crystalline component. Thus, the normal blue-shifted absorptions (from S_0 to S_1) and the new absorption at the higher energy band (from S_0 to S_c) can simultaneously be induced in the semicrystalline nanowires, as shown in Figure 2b. In the single crystalline nanosheets, the molecular excitons are all aligned in a uniformly parallel manner. All oscillator strength was associated with the strong coupled excitionic state (S_c), and thus, the original intramolecular electron transitions from the ground state to the normal excited states (from S_0 to S_1) were completely forbidden. One single narrow absorption peak (from S_0 to S_c) was thus observed at the higher energy side (Figure 2c). Furthermore, as in the normal H-aggregation, the highest energy level in the S_c bands may also hold all the oscillator strength in the single crystalline particles. Therefore, the B_c absorption peak of the nanosheets becomes stronger and exhibits a small blue-shift with respect to that of nanowires because the regular degree of molecular arrangement in the monocrystalline nanosheets may be higher than the crystalline component in semicrystalline nanowires.

To confirm further the aggregated structures and electronic states, we measured the fluorescence emission spectra of monomers, nanowires, and nanosheets (Figure 7). Although the nonemissive character of the excited state became commonly accepted as a general feature of H-aggregates, the example of a fluorescent H-aggregate composed of face-to-face stacked dyes

has recently been demonstrated.[17] In our cases, however, the emission behaviors are obviously dependent on the aggregated structures as their absorption spectra. Figure 7a,c shows that both monomers and nanosheets display only a single symmetric emission with λ_{max} at 477 and 413 nm, respectively. The highly symmetric emission and a λ_{max} difference as great as 64 nm obviously confirm that the emission of nanosheets does not originate from the blue-shift of the monomeric emission in normal aggregates but obviously originates from the higher electronic excited state in the single crystals, as illustrated in Figure 6. Interestingly, Figure 7b shows that the emission spectrum of nanowires contains one main emission peak and two shoulder peaks. The main peak with λ_{max} at 442 nm obviously results from the blue-shift (35 nm) of monomeric emission in the aggregated state because the right shoulder emission is almost at the same λ_{max} value as that of the monomers. On the other hand, the position of left shoulder emission at ~420 nm nearly approaches the emission of single crystalline nanosheets, resulting from the crystalline component in nanowires. These observations of emission behaviors further confirm that there are two kinds of electronic coupled excitonic states in the H-aggregates of coplanar organic molecules, depending on the regular degree of face-to-face stacking of molecules.

Conclusion

In summary, we have demonstrated the formation of an extremely strong coupled− excitonic interaction in H-aggregated molecular crystals by the comparison of optical behaviors between monomers and semicrystalline nanowires and monocrystalline nanosheets. One new electronic excited state with an energy band higher than that in normal H-aggregation was observed in single crystalline nanoparticles, resulting from the highly regular face-to-face stacking of molecular excitons. This higher electronic state may hold all oscillator strength, leading to the extinction of the original intramolecular electronic transitions of individual molecules and the appearance of new absorption peak and fluorescence emission at high-energy bands. The coplanar configuration of the molecular structure may play an important role in promoting the strong coupling of the molecular excitons. Although the mechanism of exciton coupling has yet to be fully understood, this present work shows a perspective that the ability to control the molecular structure and its arrangement in aggregates holds promise for creating novel optical properties in molecular materials.

Acknowledgment. This work was supported by the National Natural Science Foundation of China (60571038 and 60771036), the National 863 High Technology Project of China (2007AA10Z434), the National Basic Research Program of China (2006CB300407), the Innovation Project of Chinese Academy of Sciences (KJCX2-SW-W31), and the Basic Research Program of Anhui (07041420). We also thank the Hundreds Talent Program of the Chinese Academy of Sciences for financial support.

References and Notes

(1) Horn, D.; Rieger, J. *Angew. Chem., Int. Ed.* **2001**, *40*, 4330−4361.

(2) (a) Bertorelle, F.; Lavabre, D.; Fery-Forgues, S. *J. Am. Chem. Soc.* **2003**, *125*, 6244−6253. (b) Patra, A.; Hebalkar, N.; Sreedhar, B.; Sarkar, M.; Samanta, A.; Radhakrishnan, T. P. *Small* **2006**, *2*, 650−659. (c) Kang, L. T.; Wang, Z. C.; Cao, Z. G.; Ma, Y.; Fu, H. B.; Yao, J. N. *J. Am. Chem. Soc.* **2007**, *129*, 7305−7312.

(3) (a) An, B. K.; Kwon, S. K.; Jung, S. D.; Park, S. Y. *J. Am. Chem. Soc.* **2002**, *124*, 14410−14415. (b) Lim, S. J.; An, B. K.; Jung, S. D.; Chung, M. A.; Park, S. Y. *Angew. Chem., Int. Ed.* **2004**, *43*, 6346−6350. (c) Hu, J. S.; Guo, Y. G.; Liang, H. P.; Wan, L. J.; Jiang, L. *J. Am. Chem. Soc.* **2005**, *127*, 17090−17095. (d) Zhou, Y.; Schattka, J. H.; Antonietti, M. *Nano Lett.* **2004**, *4*, 477−481.

(4) (a) Fu, H. B.; Xiao, D. B.; Yao, J. N.; Yang, G. Q. *Angew. Chem., Int. Ed.* **2003**, *42*, 2883−2886. (b) Balakrishnan, K.; Datar, A.; Oitker, R.; Chen, H.; Zuo, J.; Zang, L. *J. Am. Chem. Soc.* **2005**, *127*, 10496−10497. (c) Balakrishnan, K.; Datar, A.; Naddo, T.; Huang, J.; Oitker, R.; Yen, M.; Zhao, J.; Zang, L. *J. Am. Chem. Soc.* **2006**, *128*, 7390−7398. (d) Datar, A.; Balakrishnan, K.; Yang, X.; Zuo, X.; Huang, J.; Oitker, R.; Yen, M.; Zhao, J.; Tiede, D. M.; Zang, L. *J. Phys. Chem. B* **2006**, *110*, 12327−12332.

(5) (a) Jelley, E. E. *Nature (London, U.K.)* **1936**, *138*, 1009−1010. (b) Fu, H. B.; Yao, J. N. *J. Am. Chem. Soc.* **2001**, *123*, 1434−1439. (c) Fu, H. B.; Loo, B. H.; Xiao, D. B.; Xie, R. M.; Ji, X. H.; Yao, J. N.; Zhang, B. W.; Zhang, L. Q. *Angew. Chem., Int. Ed.* **2002**, *41*, 962−965.

(6) (a) Emerson, E. S.; Conlin, M. A.; Rosenoff, A. E.; Norland, K. S.; Rodriguez, H.; Chin, D.; Bird, G. R. *J. Phys. Chem.* **1967**, *71*, 2396−2403. (b) Augenstein, L.; Mason, R.; Rosenberg, B. *Physical Processes in Radiation Biology*; Academic Press: New York, 1964; pp 23−42.

(7) (a) Asanuma, H.; Shirasuka, K.; Takarada, T.; Kashida, H.; Komiyama, M. *J. Am. Chem. Soc.* **2003**, *125*, 2217−2223. (b) Kashida, H.; Asanuma, H.; Komiyama, M. *Angew. Chem., Int. Ed.* **2004**, *43*, 6522−6525.

(8) Balakrishnan, K.; Datar, A.; Zhang, W.; Yang, X.; Naddo, T.; Huang, J.; Zuo, J.; Yen, M.; Moore, J. S.; Zang, L. *J. Am. Chem. Soc.* **2006**, *128*, 6576−6577.

(9) Zheng, M.; Wang, L. C.; Shao, J. G.; Zhong, Q. *Synth. Commun.* **1997**, *27*, 351−354.

(10) Masuda, H.; Yamada, H.; Satoh, M.; Asoh, H. *Appl. Phys. Lett.* **1997**, *71*, 2770−2772.

(11) (a) Steinhart, M.; Wehrspohn, R. B.; Gösele, U.; Wendorff, J. H. *Angew. Chem., Int. Ed.* **2004**, *43*, 1334−1344. (b) Steinhart, M.; Wendorff, J. H.; Greiner, A.; Wehrspohn, R. B.; Nielsch, K.; Schilling, J.; Choi, J.; Gösele, U. *Science (Washington, DC, U.S.)* **2002**, *296*, 1997. (c) Zhang, M. F.; Dobriyal, P.; Chen, J. T.; Russell, T. P. *Nano Lett.* **2006**, *6*, 1075−1079. (d) Barrett, C.; Iacopino, D.; O'Carroll, D.; Marzi, G. D.; Tanner, D. A.; Quinn, A. J.; Redmond, G. *Chem. Mater.* **2007**, *19*, 338−340.

(12) Auweter, H.; Haberkorn, H.; Heckmann, W.; Horn, D.; Lüddecke, E.; Rieger, J.; Weiss, H. *Angew. Chem., Int. Ed.* **1999**, *38*, 2188−2191.

(13) (a) Kasha, M.; Rawls, H. R.; El-Bayoumi, M. A. *Pure Appl. Chem.* **1965**, *11*, 371−393. (b) Ruban, A. V.; Horton, P.; Young, A. J. *J. Photochem. Photobiol., B* **1993**, *21*, 229−234. (c) Dähne, L.; Biller, E. *Adv. Mater.* **1998**, *10*, 241−245.

(14) (a) Li, S.; He, L.; Xiong, F.; Li, Y.; Yang, G. *J. Phys. Chem. B* **2004**, *108*, 10887−10892. (b) Tian, Z. Y.; Chen, Y.; Yang, W. S.; Yao, J. N.; Zhu, L. Y.; Shuai, Z. G. *Angew. Chem., Int. Ed.* **2004**, *43*, 4060−4063.

(15) Xiao, D. B.; Xi, L.; Yang, W. S.; Fu, H. B.; Shuai, Z. G.; Fang, Y.; Yao, J. N. *J. Am. Chem. Soc.* **2003**, *125*, 6740−6745.

(16) (a) McRae, E. G.; Kasha, M. *J. Chem. Phys.* **1958**, *28*, 721−722. (b) Norland, K.; Ames, A.; Taylor, T. *Photogr. Sci. Eng.* **1970**, *14*, 295−307. (c) Knapp, E. W. *Chem. Phys.* **1984**, *85*, 73−82.

(17) Rösch, U.; Yao, S.; Wortmann, R.; Würthner, F. *Angew. Chem., Int. Ed.* **2006**, *45*, 7026−7030.